Improved Anti-Biofouling Performance of Pressure Retarded Osmosis (PRO) by Dosing with Chlorhexidine Gluconate

Peng-Fei Sun[a], Taek-Seung Kim[a], Han-Shin Kim[a], So-Young Ham[a], Yongsun Jang[a], Yong-Gyun Park[b], Chuyang Y. Tang[c], Hee-Deung Park[a,d*]

[a] School of Civil, Environmental and Architectural Engineering, Korea University, Seoul, 02841, South Korea

[b] Environmental Process Engineering Team, GS Engineering & Construction, Seoul, 03159, South Korea

[c] Department of Civil Engineering, The University of Hong Kong, Pokfulam, Hong Kong, P.R. China

[d] KU-KIST Graduate School of Converging Science and Technology, Korea University, Seoul, 02841, South Korea

* Corresponding Author

Mailing address: School of Civil, Environmental and Architectural Engineering, Korea University, 145 Anam-Ro, Seongbuk-Gu, Seoul 02841, South Korea.

Phone : +82-2-3290-4861

FAX : +82-2-928-7656

E-mail : heedeung@korea.ac.kr

Abstract

Pressure retarded osmosis (PRO) is an emerging technology capable of extracting energy from salinity gradients of wastewater paired with SWRO brine. However, this process's performance is hindered by irreversible biofouling due to bacteria-containing wastewater and the sponge-like support layer of PRO membranes. In this study, chlorhexidine gluconate (CHG), a non-oxidizing biocide, was continuously added to feed solution to investigate its anti-biofouling performance during PRO. CHG showed higher anti-microbial and anti-biofilm activity than did other non-oxidizing biocides. Even at low dosages of CHG, water flux declines were greatly mitigated and benefited from the internal concentration polarization (ICP)-elevated concentrations within the active-support layer interface. CHG plays a critical role by inhibiting bacterial growth, and a 65-88% reduction of extracellular polymeric substances was achieved on the membrane surface and throughout the feed spacers. Membrane characterization demonstrated that the improved performance could be attributed to a consistent structural parameter and alleviation of ICP self-compensation effects. This study thus shows that a combination of biocide dosing and pressure assisted-osmotic backwashing can be a useful strategy for controlling biofouling during the PRO process.

Keywords: Pressure retarded osmosis (PRO); Biofouling; Structural parameter (*S*); Internal concentration polarization (ICP); Chlorhexidine gluconate (CHG)

1. Introduction

Increasing carbon dioxide emissions and energy consumption have invigorated and accelerated the development of new sustainable power sources. The Gibbs free energy from salinity gradients can be captured and harnessed as a promising method for renewable power production, with the potential to generate 2 TW of power [1]. Pressure-retarded osmosis (PRO) is a membrane-based technology utilized to harvest this free energy and has been intensively investigated and demonstrated to be more efficient and cost-effective than alternative technologies like reverse electrodialysis [2-6].

During PRO, the osmotic pressure difference between the low concentration feed solution and high concentration draw solution drives the pressurized permeation of water through a semipermeable membrane, which produces energy by twirling a hydro turbine. Selecting an appropriate salinity gradient is important for extracting the greatest amount of energy and improving the feasibility of PRO implementation [7]. Treated wastewater effluent paired with reverse osmosis brine is considered a promising alternative source of water owing to its relatively higher salinity gradient [8, 9]. Furthermore, using this source would enable the reutilization of numerous and diverse wastewater effluents (e.g., municipal, industrial sources). Additionally, the reverse osmosis brine can be discharged with low adverse environmental impacts owing to it is diluted by the PRO process.

However, throughout this process, membrane biofouling can be triggered by microbes ubiquitously present in impure water sources [10, 11]. Like in ultrafiltration (UF) and membrane bioreactor (MBR) processes, microorganisms initially adhere to or deposit on the membrane surface [12-14] producing a foulant layer that causes filtration resistance [15-18]. The biofilms formed on PRO membranes and spacers have been considered the main obstacle

in developing a pilot scale PRO process [19]. Additionally, the configuration required for PRO, in which the support layer faces the feed solution, radically reduces PRO performance as the permeating flow of water accelerates foulant deposition inside the porous support layer. Thus, having an unstirred layer critically impedes the reversibility of the deposited bacterial cells and their secretions [20-23]. Multiple studies have demonstrated that conventional physical flushing and osmotic backwashing do not significantly reverse biofouling [10, 24, 25]. Although modifying the membrane surface can delay the adhesion of microbes to the surface or inactivate the microbes, this strategy cannot prevent biofouling during long-term operations once membranes become covered in a fouling layer [26-29]. Therefore, it is imperative to develop new strategies for mitigating the biofouling propensity of the PRO process.

Non-oxidizing biocides act as free chlorine-suppressing agents, have better compatibility with polyamide-based membrane, and could effectively alleviate biofouling of the PRO membrane [30-32]. However, biocides are potentially harmful to organisms living in the aqueous ecological environment [33, 34]. A biocide should be carefully screened to balance effectiveness in reducing biofouling and resultant toxicity to living organisms. Additionally, the dosage and frequency should be optimized considering the organisms in the environment [30, 35]. One such non-oxidizing biocide, chlorhexidine gluconate, is a biguanide and cation-active compound that has significant antibacterial activity. As such, it has been used as an antiseptic agent and has been extensively applied in the medical field [36]. Compared with other antimicrobials or biocides, CHG exhibits broader spectrum efficacy and is able to inhibit microorganism adherence and prevent biofilm formation [37, 38]. CHG is thus a promising candidate for application in PRO for inhibition of biofilm formation and reduction of biofouling.

93 The focus of this study was to evaluate anti-biofouling activity of CHG added to the feed stream
94 of PRO. Initially, anti-microbial and anti-biofilm effects of CHG were investigated by
95 measuring the minimum inhibitory concentration (MIC) required to inhibit and the minimum
96 bactericidal concentration (MBC) to kill bacteria. Compatibility of CHG with the PRO
97 membrane was also evaluated by examining morphological and chemical damage after
98 membrane exposure to high concentrations of CHG. A series of lab-scale PRO biofouling tests
99 were then performed using different doses of biocide to evaluate the anti-biofouling potential
100 of CHG. Finally, membrane transport and structural parameters were systematically
101 determined to elucidate biofouling mitigation mechanisms when combining CHG dosing with
102 pressure-assisted osmotic backwashing (PA-OBW). To the authors' knowledge, this is the first
103 study that addresses anti-biofouling effects by directly dosing PRO process with a biocide in
104 an attempt to improve energy production.
105

2. Materials and methods

2.1. PRO membrane and synthetic solutions

A thin-film composite (TFC) osmotic membrane (CSM-PRO-4) was used in PRO biofouling tests and was provided by Toray Chemical Korea Inc. (Seoul, Korea). This membrane consisted of a polyamide (PA) active layer, a polysulfone (PS) support layer, and a fabric backing layer. The detailed intrinsic parameters and SEM images of CSM-PRO-4 membrane are summarized in the Section S1 of Supporting Information (see Table S1 and Fig. S1). Membrane samples were rinsed thoroughly and stored in deionized (DI) water at 4 °C.

Synthetic wastewater was used as the feed solution for PRO, the composition of which was modified from Bar-Zeev et al. [10]. KH_2PO_4 was replaced by KCl to prevent phosphate scaling due to internal concentration polarization (ICP) and reverse salt flux effects [8]. All synthetic wastewater components were individually dissolved in 250 mL of DI water then filtered through 0.45 μm membrane filters (Whatman, UK) and then sterilized in an autoclave to create concentrated stock solutions. Fresh synthetic wastewater was prepared by diluting the stock solutions with DI water. Additionally, for PRO, a 1.2 M NaCl solution was used as the draw solution to mimic the salinity of seawater RO brine at 50% recovery.

2.2. Bacterial strain and chemostat device

P. aeruginosa PA 14 was used as the model gram-negative bacteria for all anti-microbial, anti-biofilm, and PRO biofouling tests. Bacterial cells were cultured overnight, then washed and suspended in 50 mL of sterile synthetic wastewater for subsequent tests. A homemade chemostat device was adopted from [39] for continuous and reproducible biofilm growth during PRO biofouling tests. The final bacterial concentrations for all biofouling tests were

consistently maintained at approximately 6.5×10^5 CFU/mL. Further details of the chemostat device preparation are available in Section S1 of Supporting Information.

2.3. Biocides, anti-microbial, and anti-biofilm tests

Stock CHG solution was prepared by dissolving 20% CHG (Sigma-Aldrich) in DI water to reach the required concentration. All solutions were filtered using 0.22 μm syringe filters (Millex® filter, Carl Roth, Germany) and stored at 4 °C.

To determine the anti-microbial and bactericidal effects of CHG, the MIC and MBC were measured using broth microdilution and spread plate cultivation methods, respectively [40]. Briefly, 100 μL of biocides at concentrations ranging from 0.0625 mg/L to 32 mg/L were prepared by dilution in tryptic soy broth (TSB) (BD, Franklin Lakes, NJ, USA), then added to a 96-well microtiter plate (Sigma Aldrich). Next, 100 μL of the bacterial suspension at 6.5×10^5 CFU/mL was inoculated into each well except for the sterility control sample. The 96-well microtiter plate was then incubated at 37 °C for 24 h without agitation and the OD value of the suspended culture measured at 595 nm using an iMark microplate reader (BioRad, CA, USA). The MIC was considered the lowest concentration of CHG that inhibited bacterial growth. For MBC determination, the subsamples from the microtiter plater of MIC tests were spread on tryptic soy agar (TSA) (BD, Franklin Lakes, NJ, USA) plates and the lowest concentration of CHG that killed 99.9% of bacteria or created no visible colonies after 24 h of incubation at 37 °C was defined as the MBC. Finally, biofilm attachment on the well surfaces was evaluated by the static biofilm formation assay as previously described [41].

153 **2.4. Open-loop lab-scale PRO setup**

154 All PRO experiments were carried out in an open-loop lab-scale PRO setup (Figure S1)
155 modified from previous studies [42]. The custom-made PRO module consisted of two
156 symmetric flow channels with an exposed membrane area of 20.02 cm^2 (77 mm L × 26 mm W
157 × 1 mm H). Three tricot spacers (Spacer#1, Spacer#2, Spacer#3) were placed in the feed
158 channel, which was used in the PRO membrane module to prevent deformation from higher
159 applied pressures from the draw side [43, 44]. In addition, one diamond-shaped spacer was
160 placed in the draw side, which is commonly used in commercial spiral wound membrane
161 modules.

162

163 A 60 L feed solution was pumped using a digital gear pump (Cole-Palmer, Vernon Hills, IL,
164 USA) at a flow rate of 0.04 L/min. The feed solution from the module was directly discharged
165 to imitate an open-loop PRO system without concentration or biomass increases in the feed
166 solution. A 3 L draw solution was recirculated using a high-pressure pump (Hydra-cell pump,
167 Wanner Engineering, Minneapolis, MN) with flow rate of 0.4 L/min. The effective hydraulic
168 pressure applied to the draw side was 10 bar unless otherwise stated. The mass of the draw
169 solution was measured every 2 min using a digital balance. The temperature of both the feed
170 and draw solutions was maintained at 25.0 ± 1.0 °C. Instead of inoculating bacteria in feed
171 reservoirs, the chemostat device and a Masterflex L/S peristaltic pump (Cole-Palmer, Vernon
172 Hills, IL, USA) were used to ensure steady and continuous bacterial supplementation in the
173 inlet of PRO module for controlled biofouling studies (see Fig. S2).

174

175 **2.5. PRO biofouling and anti-biofouling tests**

176 Before PRO biofouling tests, the compatibility between CHG and the PRO membrane was
177 evaluated in accordance with our previous studies [45]. The protocol of PRO biofouling and

178 the anti-biofouling tests after application of CHG are summarized as follows. Initially, the feed
179 and draw sides were recirculated with DI water for 3 h with 10 bar of hydraulic pressure applied
180 to the draw side. After stabilization, the feed and draw solutions were replaced with fresh
181 synthetic wastewater and 1.2 M NaCl, respectively. A baseline measurement without any
182 bacterial culture or CHG was carried out to determine the dilution effect caused by permeated
183 feed solution. Following cleaning and stabilization, the biofouling experiments were initiated
184 by continuously injecting bacterial cultures into the inlet of the PRO module, followed by
185 blending with the synthetic wastewater. Biofilm was allowed to develop in the PRO module.
186 Biofouling experiments were carried out over 24 h and were terminated when the cumulative
187 permeated volume reached 450 L/m^2. The anti-biofouling experiments were performed using
188 the same procedure as the biofouling experiment but with the addition of CHG doses of either
189 0.5 mg/L or 1.0 mg/L to the feed solution reservoir. After biofouling and anti-biofouling, the
190 membrane and spacers were carefully removed from the PRO module for subsequent
191 qualitative and quantitative analysis.
192
193 Biofouling and anti-biofouling experiments were repeated in order to test membrane
194 characteristics and PA-OBW. Briefly, membranes were characterized three times: before and
195 after the biofouling tests (Pristine and Biofouled conditions, respectively) and at the end of PA-
196 OBW (Cleaned condition). PA-OBW was conducted by replacing the feed solution with
197 SWRO brine (1.2 M NaCl) and replacing the draw solution with DI water while maintaining
198 10 bar of hydraulic pressure at the draw side [21]. PA-OBW was carried out for 1 h and
199 terminated by switching both feed and draw solutions with solutions of the initial configuration.
200 Water flux recovery of cleaned PRO membrane was then determined to compare biofouling
201 reversibility and cleaning efficiency with and without CHG dosing.
202

An additional control experiment was also performed by dosing with CHG and without bacterial injection to evaluate the adverse effects of CHG on the operational performance of the PRO process.

2.6. Biofilm characterization

At the end of each biofouling and anti-biofouling experiment, the biofouled membrane was immediately removed from the PRO module and divided into two subsamples for analysis using confocal laser scanning microscopy (CLSM) and other quantitative tests. The detailed analytical procedures are available in Section S2 of Supporting Information.

2.7. Membrane characterization

The water permeability, salt permeability, and structural parameters of PRO membranes were characterized using a newly developed method based on modifications of the single FO method [46]. The tests were performed in four stages using different concentrations of draw solution (0.4 M, 0.7 M, 1.0 M, and 1.3 M NaCl) and DI water for the feed solution. The water flux (J_w) was calculated from the weight changes in draw solution using a scale while the reverse salt flux (J_s) was determined by measuring increases in the rate of feed solution conductivity according to the mass balance. At each stage, at the addition of concentrated NaCl stock solution, the flow rate of the draw side was elevated to 1.2 L/min to accelerate the system to a steady state; then, the membrane was tested at least for 20 min. Eight transport equations (one for water flux and one for solute flux at each draw solution concentration) and three unknowns (A, B, S) were generated which constitute an over-determined non-linear system using the following water and salt flux governing equations developed for PRO:

$$J_w = A\left\{\frac{\pi_{D,b}\exp\left(-\frac{J_w}{k}\right)-\pi_{F,b}\exp\left(\frac{J_w S}{D}\right)}{1+\frac{B}{J_w}\left[\exp\left(\frac{J_w S}{D}\right)-\exp\left(-\frac{J_w}{k}\right)\right]}-\Delta P\right\}, \text{ and} \quad (1)$$

$$J_s = B\left\{\frac{C_{D,b}\exp\left(-\frac{J_w}{k}\right)-C_{F,b}\exp\left(\frac{J_w S}{D}\right)}{1+\frac{B}{J_w}\left[\exp\left(\frac{J_w S}{D}\right)-\exp\left(-\frac{J_w}{k}\right)\right]}\right\}, \quad (2)$$

where $C_{F,b}$ and $\pi_{F,b}$ are the solute concentration and osmotic pressure of the feed solution, respectively, and $C_{D,b}$ and $\pi_{D,b}$ are the solute concentration and osmotic pressure of the draw solution, respectively. In addition, k is the mass transfer coefficient, D is the diffusion coefficient of the feed side, and ΔP is the applied hydraulic pressure on the draw side.

The least-squares method was used to minimize global errors between experimental values and calculated fluxes [47]. This algorithm was carried out using Microsoft Excel office 365 (Microsoft Corporation, Redmond, WA) with the solver function and A, B, and S were calculated automatically to yield an optimal solution.

2.8. Statistical analysis

The statistical analysis was carried out with Statistical Package for the Social Science (IBM SPSS) software. *P*-values were estimated using the independent samples *t*-test to determine statistically significant differences at 95% or 99.5% confidence intervals ($P < 0.05$, or $P < 0.005$).

3. Results and discussion

3.1. Anti-microbial and anti-biofilm effects of CHG

During static biofilm formation tests, bacterial growth of *P. aeruginosa* was inhibited at CHG concentrations above 4 mg/L and significantly controlled when the CHG concentration was above the MIC of 8 mg/L (Fig. 1a). CHG also exhibited effective inhibition of biofilm formation at relatively lower concentrations (Fig. 1b). It is worth noting that CHG exhibited relatively low MIC and MBC values for gram-positive bacteria like *S. aureus* (Fig. S3). These results indicate that CHG possesses high anti-microbial activity and that relatively low concentrations of CHG are capable of inhibiting or killing bacteria compared to other biocides (Table S2).

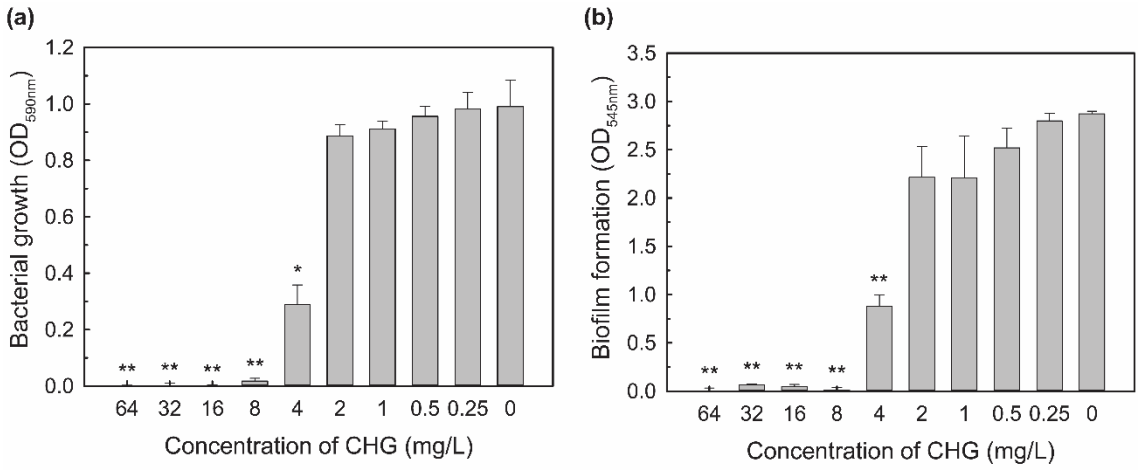

Fig. 1. Anti-microbial and anti-biofilm effects of CHG treatment. (a) Growth inhibition of *P. aeruginosa* by CHG treatment. (b) Effect of CHG treatment on of *P. aeruginosa* biofilm formation. Error bars indicate the standard deviations of six measurements. *, $P < 0.05$ versus the control; **, $P < 0.005$ versus the control.

Under the flow regimes, variations in biofilm structure and the viability of bacterial cells on PRO membranes were investigated by using a drip flow reactor. CLSM images (Fig. S4a to e) indicate that the amount of inactivated or dead cells increased after dosing of the feed reservoir with biocide. In addition, increasing the concentration of CHG from 1 mg/L to 8 mg/L led to

significant reductions in biovolume and average thickness from 86.2% to 18.2% and from 83.8% to 29.6%, respectively (Fig. S4f).

Unlike other biocides like DBNPA, which causes inactivation of ATPases in the cell membrane, CHG is rapidly taken up by bacteria and is more inclined to collapse membrane potential at lower concentrations [36], which may explain why CHG has higher anti-microbial activity than other biocides. Although previous studies [38, 48] have demonstrated that bacterial surfaces are more hydrophobic after CHG treatment, because the hexamethylene hydrophobic chain of the CHG biguanide is constrained at the cell surface, it remains controversial whether this hydrophobicity interferes with bacterial adhesion [49, 50]. Biofilm formation and structure are also influenced by other variables, like bacterial viability, EPS matrix composition, and membrane properties. With CHG treatment, the EPS substances may be altered and more susceptible to shear stress, resulting in a delay in initial adhesion and biofilm formation.

3.2. Effects of CHG on membrane and PRO performance

Before evaluating potential adverse effects of CHG on PRO performance, compatibility between CHG and the PRO membrane was assessed. Fig. S5a shows SEM images of the membrane active layer after immersion in CHG (50,000 mg/L), NaOCl (50,000 mg/L), or DI water for 1 h. After treatment of the PRO membrane with 50,000 mg/L CHG, no apparent change in surface morphology was observed. In contrast, after treatment with 50,000 mg/L of NaOCl solution, the active layer became smoother and the “ridge-valley” structure mostly disappeared. The NaOCl-treated PRO membrane showed depressions at 1541 and 1663 cm^{-1} compared to DI-treated PRO membranes (Fig. S5b), indicating damage of N-H and C=O bonds after the hydrogen of amide II was replaced by chlorine through electrophilic substitution in N-chlorination [51, 52]. However, similar absorbance peaks at the characteristic wavelengths

were observed from the CHG-treated and DI-treated PRO membranes. These results suggest that CHG is compatible with the PRO membrane.

PRO performance tests were then performed using bacteria-free synthetic wastewater containing various concentrations of CHG as the feed solution. For baseline tests without CHG, the flux curve showed almost no drop when the permeate volume reached 450 L/m^2 (Fig. 2a). With increasing concentrations of CHG, the water flux decline was increasingly severe relative to baseline flux. Normalized water flux was plotted as a function of accumulated CHG load and is shown in Fig. 2b. Flux showed almost no decrease (J_w/J_0 = 96-98%) with the initial CHG load of 300 mg/m^2. However, a critical decline in flux (J_w/J_0 = 62-65%) was observed with increasing CHG load up to 700 mg/m^2, at which point flux levels appeared to stabilize. Fig. 2b shows that the extent of flux decline was independent of CHG concentration for a given amount of accumulated CHG. This may be because CHG is an organic compound that continuously accumulates across the membrane surface and can penetrate into the support layer with permeated water flow [53]. Results from these evaluations were helpful in conducting subsequent anti-biofouling experiments and suggested that CHG should be used at relatively low concentrations.

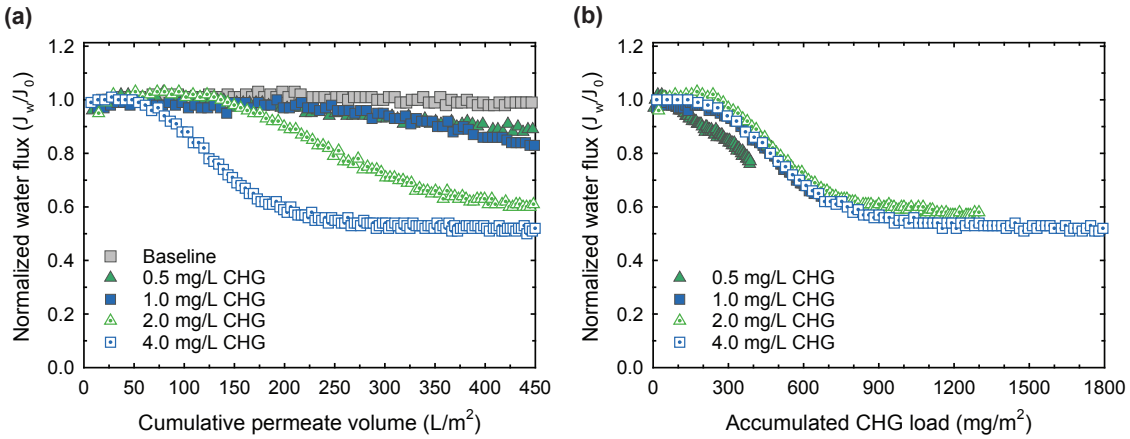

Fig. 2. Comparison of water flux behavior induced by continuous treatments with different concentrations of CHG. (a) Normalized water flux as a function of cumulative

permeated water volume. (b) Normalized water flux as a function of accumulated CHG loading. The accumulated CHG load (mg/m^2) was the product of cumulative permeated volume (L/m^2) and the concentration of CHG (mg/L). All experiments performed without bacterial inoculation.

3.3. Anti-biofouling performance of CHG

3.3.1. Effects of CHG on water flux recovery

A series of anti-biofouling experiments were conducted in our open-loop lab-scale PRO process (Fig. S2) to evaluate the ability of CHG to mitigate water flux decline. In light of previous studies [10], multiple measures have been taken to improve the reliability of such experiments. The configuration of the PRO module was re-designed to mimic the pilot PRO module. Moreover, relatively consistent levels and concentrations of bacterial culture from a chemostat (Fig. S6) were continuously injected to the PRO system, ensuring that feed solution conditions were identical in physiochemical and biological properties, and that biofilms could be reproducibly formed on the membrane surface or inside support layer.

Initial water flux for all experiments was ~20 LMH, which was achieved by using identical osmotic pressure differences ($\Delta\pi$ = 49 bar), applied hydraulic pressures (ΔP = 10 bar), crossflow velocities, and bacterial concentrations (6.5×10^5 CFU/mL). Fig. 3 shows the marked differences in normalized permeate flux decline that occurred with and without the addition of CHG. Without CHG, the permeate flux decreased to ~31% of the initial flux. CHG doses of 0.5 mg/L and 1.0 mg/L of CHG caused permeate flux to decrease to ~80% and ~65% of initial levels, respectively, which clearly demonstrate the effect of CHG on mitigating biofouling. The lower levels of water flux recovery after using 1.0 mg/L CHG compared to 0.5 mg/L CHG may be due to additional adverse effects of high concentrations of CHG, whose accumulation in the porous support can also cause a reduction in permeate flux (see Fig. 2).

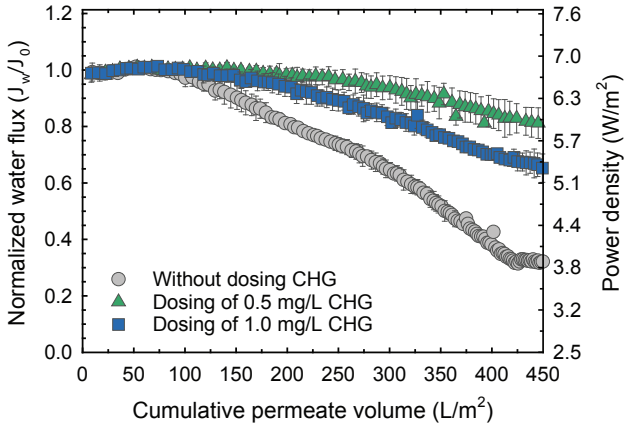

Fig. 3. Effect of treatments with different concentration of CHG on water flux decline. Feed solutions were prepared with the desired concentration of CHG. All experiments were performed with inoculations of 6.5×10^5 CFU/mL of bacteria. Error bars indicate the standard deviations from three independent experiments.

The most stable PRO performance was achieved at a CHG dosage of 0.5 mg/L even though this concentration was much lower than the MIC. The high efficacy of CHG in retarding biofouling even at concentrations below the MIC can be explained by internal concentration polarization (ICP) of CHG in the porous substrate of the membrane [22], which may have resulted in an actual concentration of CHG in the membrane substrate that was much higher than that of the bulk solution. Although ICP is generally considered to be an undesirable phenomena associated with loss of osmotic driving force and more severe membrane fouling [25, 54, 55], the current study reveals the possibility of taking advantage of ICP to achieve reduced chemical dosing for biofouling control. Based on this mechanism, a lower CHG dosage is advantageous for controlling biofouling due to the potential cost savings for PRO operation and lower levels of adverse effects on PRO water flux.

3.3.2. Analysis of biofilm formation on membrane surfaces and feed spacers

Fig. 4 shows biofilm formation on the surface of the membrane support layer. Due to the water permeating through the open pores of the porous fabric backing layer, biofilms predominantly formed around these openings, as reported previously [10]. Similar to the RO membranes [56],

PRO membranes were compacted and deformed in a weave-like pattern at an applied hydraulic pressure of 10 bar. Consequently, biofilm morphologies were irregular and were consistent with the shapes of the membrane and tricot spacer (Fig. S7). Without CHG, biofilms appeared to cover the entire membrane surface (Fig. 4a). In contrast, when CHG was present, biofilm distributions were loose, patchy, and non-continuous, and biofilms were rarely formed on areas with close contact to spacer filaments (Fig. 4b, Fig. S7). Table 1 shows that the biofilm average thickness was 29.0 ± 2.5 μm without CHG and was nearly 4-fold and 13-fold thicker than those treated with 0.5 mg/L and 1.0 mg/L CHG, respectively. In addition, the biovolume on the surface of the membrane support layer was greatly decreased by the presence of CHG (Table 1). Previous studies have demonstrated that bacteria could penetrate the support layer and cause severe biofouling [10, 42]. Therefore, the efficiency of dosing with CHG throughout the cross-section for controlling biofouling should be appropriately observed by CLSM in future studies [57].

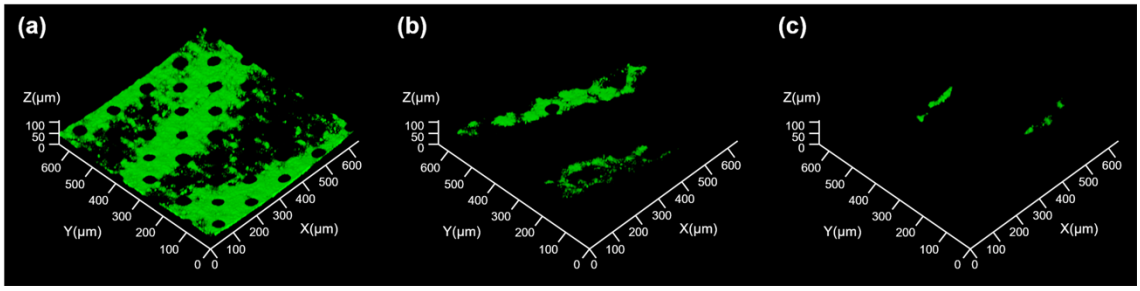

Fig. 4. 3-D CLSM images of biofilm development on the surface of the PRO membrane support layer. (a) Biofilm formation without CHG treatment. (b) Biofilm formation mitigation by 0.5 mg/L CHG. (c) Biofilm formation mitigation by 1.0 mg/L CHG.

Table 1. Comparisons of biomass and biofilm thickness on membrane surfaces treated with different concentration of CHG.

Experimental Groups	Biovolume [a] ($\mu m^3/\mu m^2$)	Thickness [a] (μm)
Without dosing CHG	23.7 ± 3.3	29.0 ± 2.5
Dosing of 0.5 mg/L	6.8 ± 2.3 [b]	8.5 ± 3.1 [b]
Dosing of 1.0 mg/L	1.8 ± 0.6	2.2 ± 0.6 [b]

[a] Biovolume and thickness were averaged, with standard deviation (SD) calculated from five random subsamples of CLSM images.
[b] Indicates significant differences with and without CHG treatment, $P < 0.05$.

Fig. 5 shows quantitative analysis of extracellular polymeric substrate (EPS) coverage, viable cell coverage, and total organic carbon (TOC) coverage of biofilms accumulated on the surface of PRO membranes and feed spacers. Generally, the total EPS (protein and polysaccharide) on membrane surfaces decreased from 20.8 μg/cm^2 to 6.1 μg/cm^2 and 2.4 μg/cm^2 after treatment with either 0.5 mg/L or 1.0 mg/L of CHG, respectively. Meanwhile, EPS levels throughout the feed spacers (Spacer#1, Spacer#2, and Spacer#3) were reduced by ~65%-80% in the presence of CHG. Additionally, almost 98% of cells on the membrane surface were inactivated (Fig. 5b) and TOC coverage was reduced to ~20%-35% by a 0.5 mg/L dose of CHG compared to the control group (Fig. 5c).

Interestingly, when the EPS values were normalized by the number of viable cells (EPS/cell), normalized EPS values increased with increasing CHG dose compared to control conditions, especially in the feed spacers (5.0 and 2.4 for 0.5 mg/L and 1.0 mg/L of CHG, respectively, versus to 0.2 for controlled group). We speculated that EPS coverage increased as viable bacteria exhibited resistance to lower dosages of biocides. Nevertheless, as a benefit to the significant decreases in the amount of cell adhesion to membrane surfaces, the total biomass and EPS were substantially reduced at the CHG dose concentration of 0.5 mg/L compared to 1.0 mg/L. Moreover, the protein to polysaccharide ratio (PN/PS) was slightly elevated in the presence of CHG (see Fig. S8), suggesting that the dicationic CHG molecules interact with the anionic carboxylate groups of EPS [38] and may alter the biofilm composition.

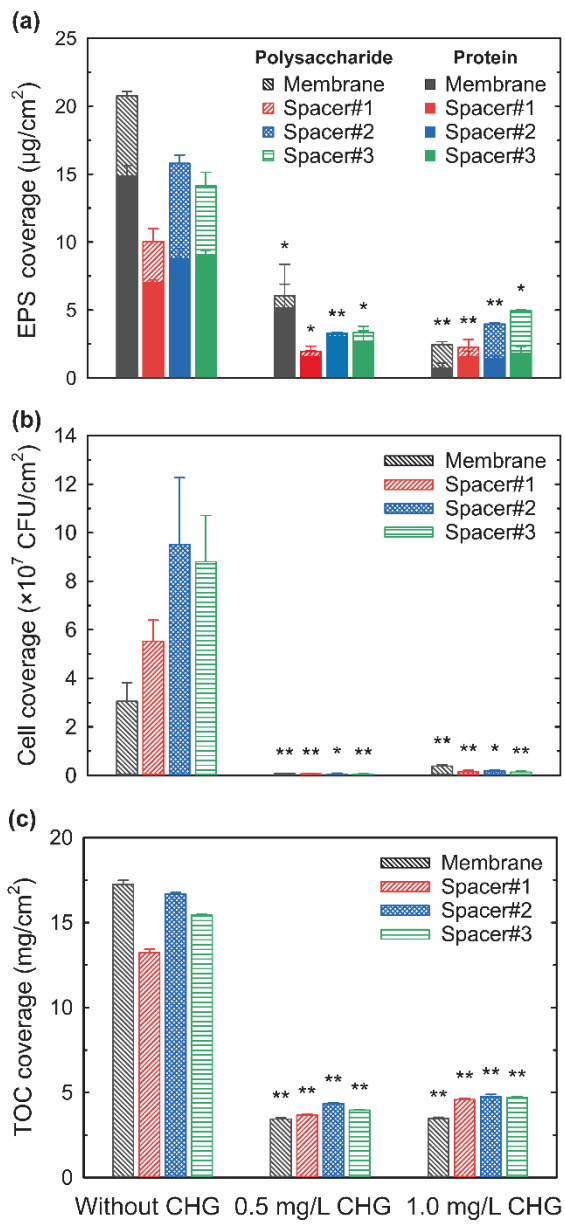

Fig. 5. Comparison of biofilm properties and biomass changes on membrane surfaces and in feed spacers with and without CHG treatment. (a) Variations of EPS composition (proteins and polysaccharides), (b) cell coverage, and (c) TOC coverage. Error bars indicate standard deviations of four measurements. *, $P < 0.05$ versus the control, **, $P < 0.005$ versus the control.

3.3.3. Improved water flux recovery by combining CHG treatment with PA-OBW

Previous studies [21, 54] have demonstrated that backwashing is an effective way to recover water flux after organic and inorganic fouling; however, biofouling within the support layer of PRO membranes eclipses the impact of osmotic backwashing and detrimentally impedes power

generation [10]. Results of our anti-biofouling experiments indicate that PRO membrane biofouling is greatly alleviated by CHG treatments, allowing for increased operation time. We propose that combining CHG treatments with PA-OBW may result in performance recovery and improve the feasibility of PRO at the pilot and larger scales.

Fig. 6 shows water flux decline after biofouling with and without CHG treatments and flux recovery after PA-OBW. First, CHG treatments enabled flux maintenance at higher levels during biofouling tests, similar to results of section 3.3.1. After PA-OBW, considerable water flux recovery was observed when performed in conjunction with CHG treatments (~89% and ~82% for the 0.5 mg/L and 1.0 mg/L CHG groups, respectively, Fig. 6a), whereas only ~42% water flux was recovered without CHG treatment. Note that the water flux of cleaned membranes without CHG treatment gradually declined at a higher rate, indicating that the unrestricted growth of bacteria on the membrane surfaces and within the support layer enables the reoccurrence of severe biofouling. These results thus demonstrate that biofouling occurs during PRO and can be effectively mitigated by CHG treatments and quick osmotic backwashing.

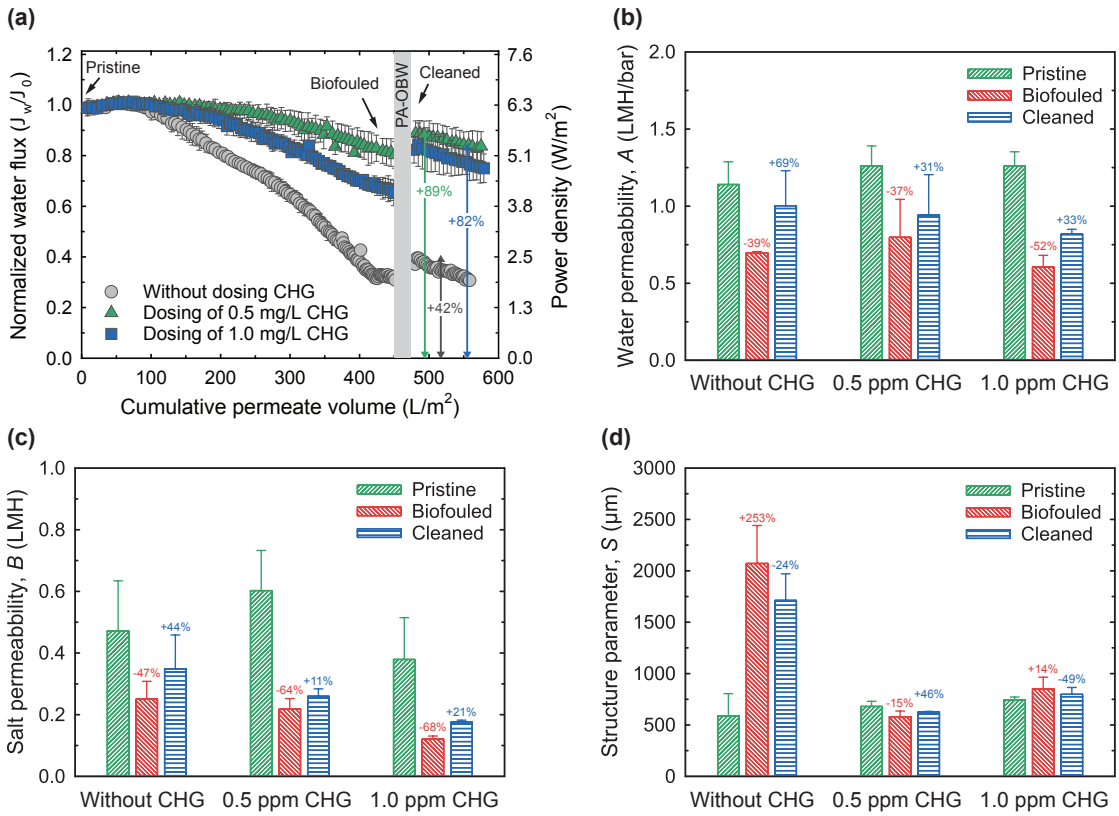

Fig. 6. Comparison of water flux recovery and membrane parameters with and without CHG treatment. (a) Normalized water flux decline with (red circle for 0.5 mg/L, blue triangle for 1.0 mg/L) and without (dark square) CHG treatment as a function of the cumulative permeating volume. PA-OWB was conducted when the permeated volume reached 450 L/m^2. Percentages indicate water flux recovery ($(J_C\text{-}J_B)/(J_P\text{-}J_B)$) after cleaning. (b) Water permeability, (c) salt permeability, and (d) structural parameters of PRO membranes were determined at three stages: before the biofouling (pristine, green), after biofouling (biofouled, red), and after PA-OBW (cleaned, blue). The red number labels indicate changes ($(i_B\text{-}i_P)/i_P$) relative to the pristine membrane while the blue number labels refer to recovery ($(i_C\text{-}i_B)/(i_P\text{-}i_B)$). Parameter values (*A, B,* and *S*) are indicated by *i*. Error bars indicate the standard deviations from three independent experiments.

3.4. Mechanisms and implications of PRO biofouling control

Characteristic transport and structural parameters of pristine and biofouled membranes (Fig. 6, green and red columns, respectively) were systematically determined and compared. Generally, water permeability (*A*) and apparent salt permeability (*B*) were decreased after biofouling in all experiments (Figure 6b, 6c). At the same time, the structure parameter (*S*) of biofouled membranes dramatically increased without CHG treatment (+253% relative to a pristine

membrane) and remained nearly constant with CHG treatment (-15% and +14% with 0.5 mg/L and 1.0 mg/L CHG treatments, respectively, Fig. 6d).

In the absence of CHG, the unrestricted proliferation of cell clusters and EPS secretions in the porous support layer leads to increased tortuosity (τ) and decreased porosity (ε), causing substantial increases in S ($S = \tau \cdot l/\varepsilon$, [58]). This prevented easy diffusion of convective salt from the feed side to restore concentrations to those of the bulk feed solution [21]. As a result, ICP was greatly enhanced and the effective osmotic pressure difference ($\Delta\pi_{eff}$, Fig. 7a) was significantly reduced, leading to lower water flux (~31% versus initial flux) and lower power density (~1.96 W/m^2). In the presence of CHG, we speculate that cell clusters may be mostly inhibited by ICP-elevated higher concentrations of CHG (~3.3-6.5 mg/L, close to the MIC) within the support layer and the active-support layer interface. Despite the decline in A, the near lack of change in S and reduced B were more favorable for achieving higher $\Delta\pi_{eff}$ (see Fig. 7c). Consequently, the water flux and power density could be maintained at relatively high levels (~80% and ~65% of initial flux and ~5.1 W/m^2 and ~4.2 W/m^2 after treatment with 0.5 mg/L or 1.0 mg/L CHG, respectively).

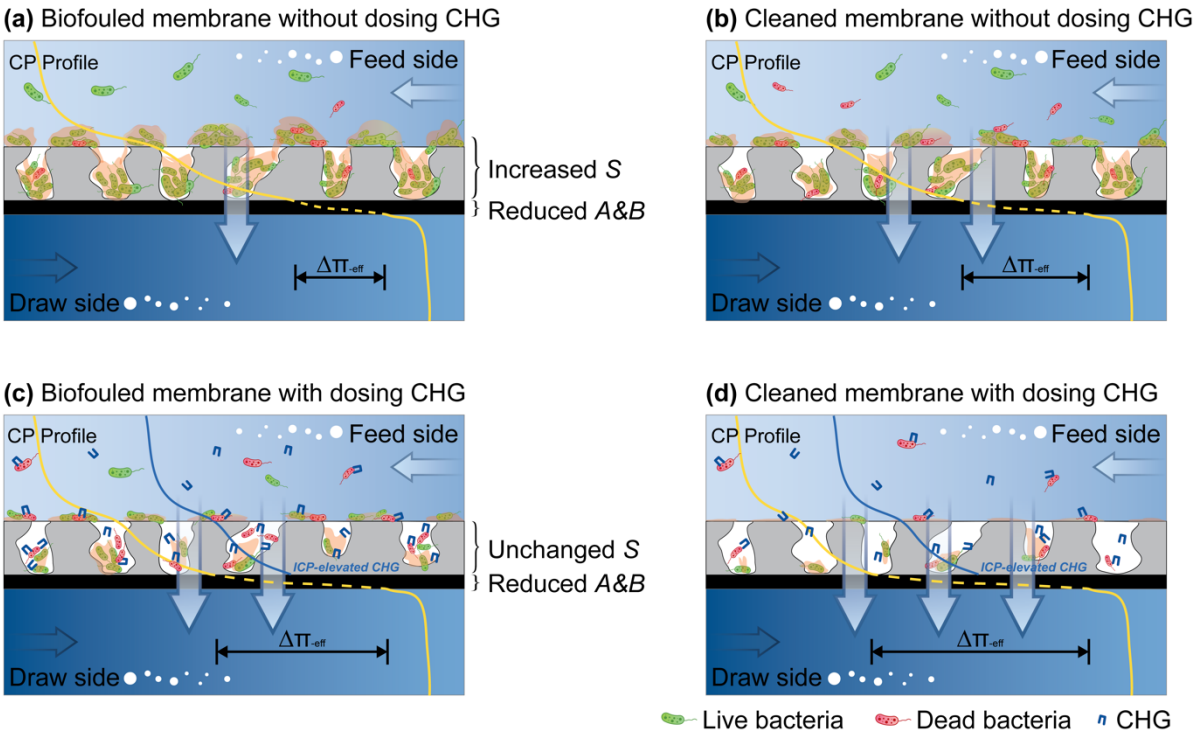

Fig. 7. Conceptual diagrams of the biofouling behaviors and the control mechanisms of CHG treatment. (a) and (c) Biofouled membranes without and with CHG treatment, respectively; (b) and (d) Cleaned membranes after rigorous PA-OBW, without and with CHG treatments, respectively.

The parameters of cleaned membranes (Fig. 6, blue columns) after PA-OBW in all experimental groups were also characterized. It is interesting to note that the *S* values of the cleaned membranes without CHG treatment was 3-fold (>1700 μm) higher than that of pristine membranes, while the *S* values remained practically unchanged (~700 μm) after backwashing in the presence of CHG (Fig. 6d). In addition, the sensitivity analysis results demonstrated that the beneficial effects of recovered *A* are mostly compromised when *S* remains high (Fig. S8).

Similar to the ICP self-compensation effect [58, 59], the biofouled membrane without CHG treatment has a higher *S*, which leads to severe ICP levels. Thus, more external efforts need to be taken to elevate the $\Delta\pi$ due to the recovery in water flux accompanied by increased adverse impacts of ICP (see equation 1). However, the biofouled membranes treated with CHG had

lower *S* values and the milder ICP has a less detrimental effect on $\Delta\pi$ recovery. After identical PA-OBW treatments, the looser, thinner, and moribund biofilm on and within support layers can be removed, making the cleaned membrane more accessible to enhance water flux and improve power density.

In our study, we found a beneficial use of the traditionally undesirable phenomenon of ICP of CHG in the porous support layer to achieve higher anti-biofilm efficiency at relatively low biocide dosage. In addition, we revealed that the enhanced maintenance of the *S* value in the presence of CHG was the principal mechanism of improved anti-biofouling performance. The combination of biocide dosing with quick PA-OBW has provided insights into practical biofouling control strategies and helped achieve encouraging performance recovery. Although the CHG anti-biofouling performance tests were conducted with an on-line continuous dosing model in our lab-scale PRO process, for larger scale or long-term operation of PRO, the dosing mode (intermittent, on-line shock/continuous, or off-line clean-in-place), dosing frequency, and cost-benefit analysis of biocide use should be systematically optimized. Future studies are needed to alleviate the adverse effects of CHG on membrane performance, to reduce chemical usage, and to mitigate adverse environment impacts.

4. Conclusions

In the current study, systematic approaches were developed to evaluate a non-oxidizing biocide for biofouling control. It was found that the non-oxidizing biocide CHG showed higher anti-microbial and anti-biofilm effects than other biocides and was compatible with the PRO membrane. CHG plays a critical role in PRO by inhibiting bacterial growth and reducing EPS secretions on both the membrane surface and feed spacers. In addition, even low dosages of CHG improved anti-biofouling performance and reduced adverse effects on water flux, which benefited from the ICP effect that elevated the concentration of CHG within the active-support layer interface. This study also shows that the predominant role of S is not significantly changed due to greatly alleviated biofouling upon CHG treatment, thus weakening the ICP self-compensation effect. By combining CHG treatment with PA-OBW, higher water flux recovery and comparable power density is possible with the PRO process.

Acknowledgments

This research was supported by funds from the Ministry of Land, Infrastructure and Transport (16IFIP-B065893-04). The authors also thank Toray Chemical Korea Inc. for supplying the PRO membranes.

Appendix A. Supporting Information

References

[1] B.E. Logan, M. Elimelech, Membrane-based processes for sustainable power generation using water, Nature, 488 (2012) 313-319. https://doi.org/10.1038/nature11477

[2] A. Achilli, T.Y. Cath, A.E. Childress, Power generation with pressure retarded osmosis: An experimental and theoretical investigation, J. Membr. Sci., 343 (2009) 42-52. https://doi.org/10.1016/j.memsci.2009.07.006

[3] B.J. Feinberg, G.Z. Ramon, E.M. Hoek, Thermodynamic analysis of osmotic energy recovery at a reverse osmosis desalination plant, Environ. Sci. Technol., 47 (2013) 2982-2989. https://doi.org/10.1021/es304224b

[4] A.P. Straub, S. Lin, M. Elimelech, Module-scale analysis of pressure retarded osmosis: Performance limitations and implications for full-scale operation, Environ. Sci. Technol., 48 (2014) 12435-12444. https://doi.org/10.1021/es503790k

[5] G.Z. Ramon, B.J. Feinberg, E.M.V. Hoek, Membrane-based production of salinity-gradient power, Energy Environ. Sci., 4 (2011) 4423-4434. https://doi.org/10.1039/c1ee01913a

[6] N.Y. Yip, M. Elimelech, Comparison of energy efficiency and power density in pressure retarded osmosis and reverse electrodialysis, Environ. Sci. Technol., 48 (2014) 11002-11012. https://doi.org/10.1021/es5029316

[7] A.P. Straub, A. Deshmukh, M. Elimelech, Pressure-retarded osmosis for power generation from salinity gradients: is it viable?, Energy Environ. Sci., 9 (2016) 31-48. http://dx.doi.org/10.1039/C5EE02985F

[8] D.I. Kim, J. Kim, H.K. Shon, S. Hong, Pressure retarded osmosis (PRO) for integrating seawater desalination and wastewater reclamation: Energy consumption and fouling, J. Membr. Sci., 483 (2015) 34-41. https://doi.org/10.1016/j.memsci.2015.02.025

[9] C.F. Wan, T.-S. Chung, Osmotic power generation by pressure retarded osmosis using seawater brine as the draw solution and wastewater retentate as the feed, J. Membr. Sci., 479 (2015) 148-158. https://doi.org/10.1016/j.memsci.2014.12.036

[10] E. Bar-Zeev, F. Perreault, A.P. Straub, M. Elimelech, Impaired performance of pressure-retarded osmosis due to irreversible biofouling, Environ. Sci. Technol., 49 (2015) 13050-13058. https://doi.org/10.1021/acs.est.5b03523

[11] R. Valladares Linares, S.S. Bucs, Z. Li, M. AbuGhdeeb, G. Amy, J.S. Vrouwenvelder, Impact of spacer thickness on biofouling in forward osmosis, Water Res., 57 (2014) 223-233. https://doi.org/10.1016/j.watres.2014.03.046

[12] J. Teng, L. Shen, Y. He, B.-Q. Liao, G. Wu, H. Lin, Novel insights into membrane fouling in a membrane bioreactor: Elucidating interfacial interactions with real membrane surface, Chemosphere, 210 (2018) 769-778. https://doi.org/10.1016/j.chemosphere.2018.07.086

[13] Z. Zhao, Y. Lou, Y. Chen, H. Lin, R. Li, G. Yu, Prediction of interfacial interactions related with membrane fouling in a membrane bioreactor based on radial basis function artificial neural network (ANN), Bioresour. Technol., 282 (2019) 262-268. https://doi.org/10.1016/j.biortech.2019.03.044

[14] J. Teng, M. Zhang, K.T. Leung, J. Chen, H. Hong, H. Lin, B.Q. Liao, A unified thermodynamic mechanism underlying fouling behaviors of soluble microbial products (SMPs) in a membrane bioreactor, Water Res., 149 (2019) 477-487. https://doi.org/10.1016/j.watres.2018.11.043

[15] M. Zhang, H. Hong, H. Lin, L. Shen, H. Yu, G. Ma, J. Chen, B.Q. Liao, Mechanistic insights into alginate fouling caused by calcium ions based on terahertz time-domain spectra analyses and DFT calculations, Water Res., 129 (2018) 337-346. https://doi.org/10.1016/j.watres.2017.11.034

[16] S. Shao, Y. Wang, D. Shi, X. Zhang, C.Y. Tang, Z. Liu, J. Li, Biofouling in ultrafiltration process for drinking water treatment and its control by chlorinated-water and pure water backwashing, Sci. Total Environ., 644 (2018) 306-314. https://doi.org/10.1016/j.scitotenv.2018.06.220
[17] R. Li, Y. Lou, Y. Xu, G. Ma, B.-Q. Liao, L. Shen, H. Lin, Effects of surface morphology on alginate adhesion: Molecular insights into membrane fouling based on XDLVO and DFT analysis, Chemosphere, 233 (2019) 373-380. https://doi.org/10.1016/j.chemosphere.2019.05.262
[18] Y. Chen, J. Teng, L. Shen, G. Yu, R. Li, Y. Xu, F. Wang, B.Q. Liao, H. Lin, Novel insights into membrane fouling caused by gel layer in a membrane bioreactor: Effects of hydrogen bonding, Bioresour. Technol., 276 (2019) 219-225. https://doi.org/10.1016/j.biortech.2019.01.010
[19] A. Bogler, S. Lin, E. Bar-Zeev, Biofouling of membrane distillation, forward osmosis and pressure retarded osmosis: Principles, impacts and future directions, J. Membr. Sci., 542 (2017) 378-398. https://doi.org/10.1016/j.memsci.2017.08.001
[20] D.I. Kim, J. Kim, S. Hong, Changing membrane orientation in pressure retarded osmosis for sustainable power generation with low fouling, Desalination, 389 (2016) 197-206. https://doi.org/10.1016/j.desal.2016.01.008
[21] N.Y. Yip, M. Elimelech, Influence of natural organic matter fouling and osmotic backwash on pressure retarded osmosis energy production from natural salinity gradients, Environ. Sci. Technol., 47 (2013) 12607-12616. https://doi.org/10.1021/es403207m
[22] M. Zhang, D. Hou, Q. She, C.Y. Tang, Gypsum scaling in pressure retarded osmosis: Experiments, mechanisms and implications, Water Res., 48 (2014) 387-395. https://doi.org/10.1016/j.watres.2013.09.051
[23] X. Song, Z. Liu, D.D. Sun, Nano gives the answer: Breaking the bottleneck of internal concentration polarization with a nanofiber composite forward psmosis membrane for a high water production rate, Adv. Mater., 23 (2011) 3256-3260. https://doi.org/10.1002/adma.201100510
[24] H. Yoon, Y. Baek, J. Yu, J. Yoon, Biofouling occurrence process and its control in the forward osmosis, Desalination, 325 (2013) 30-36. https://doi.org/10.1016/j.desal.2013.06.018
[25] G. Han, J. Zhou, C. Wan, T. Yang, T.S. Chung, Investigations of inorganic and organic fouling behaviors, antifouling and cleaning strategies for pressure retarded osmosis (PRO) membrane using seawater desalination brine and wastewater, Water Res., 103 (2016) 264-275. https://doi.org/10.1016/j.watres.2016.07.040
[26] X. Liu, L.X. Foo, Y. Li, J.Y. Lee, B. Cao, C.Y. Tang, Fabrication and characterization of nanocomposite pressure retarded osmosis (PRO) membranes with excellent anti-biofouling property and enhanced water permeability, Desalination, 389 (2016) 137-148. https://doi.org/10.1016/j.desal.2016.01.037
[27] D.L. Zhao, S. Das, T.-S. Chung, Carbon quantum dots grafted antifouling membranes for osmotic power generation via pressure-retarded osmosis process, Environ. Sci. Technol., 51 (2017) 14016-14023. https://doi.org/10.1021/acs.est.7b04190
[28] D. Zhao, G. Qiu, X. Li, C. Wan, K. Lu, T.S. Chung, Zwitterions coated hollow fiber membranes with enhanced antifouling properties for osmotic power generation from municipal wastewater, Water Res., 104 (2016) 389-396. https://doi.org/10.1016/j.watres.2016.08.045
[29] X. Li, T. Cai, T.-S. Chung, Anti-fouling behavior of hyperbranched polyglycerol-grafted poly(ether sulfone) hollow fiber membranes for osmotic power generation, Environ. Sci. Technol., 48 (2014) 9898-9907. https://doi.org/10.1021/es5017262
[30] U. Bertheas, K. Majamaa, A. Arzu, R. Pahnke, Use of DBNPA to control biofouling in RO systems, Desalin. Water Treat., 3 (2009) 175-178. https://doi.org/10.5004/dwt.2009.457

[31] T.S. Kim, H.D. Park, Tributyl tetradecyl phosphonium chloride for biofouling control in reverse osmosis processes, Desalination, 372 (2015) 39-46. https://doi.org/10.1016/j.desal.2015.06.019
[32] T.S. Kim, M. Antoinette, H.D. Park, Combination of lauroyl arginate ethyl and nisin for biofouling control in reverse osmosis processes, Desalination, 428 (2018) 12-20. https://doi.org/10.1016/j.desal.2017.11.017
[33] J.R. Lawrence, B. Zhu, G.D.W. Swerhone, E. Topp, J. Roy, L.I. Wassenaar, T. Rema, D.R. Korber, Community-Level Assessment of the Effects of the Broad-Spectrum Antimicrobial Chlorhexidine on the Outcome of River Microbial Biofilm Development, Appl. Environ. Microbiol., 74 (2008) 3541-3550. https://doi.org/10.1128/AEM.02879-07
[34] L. Coquet, A. Obry, N. Borghol, J. Hardouin, L. Mora, A. Othmane, T. Jouenne, Impact of chlorhexidine digluconate and temperature on curli production in *Escherichia coli*-consequence on its adhesion ability, AIMS microbiology, 3 (2017) 915-937. https://doi.org/10.3934/microbiol.2017.4.915
[35] K. Majamaa, J.E. Johnson, U. Bertheas, Three steps to control biofouling in reverse osmosis systems, Desalin. Water Treat., 42 (2012) 107-116. https://doi.org/10.1080/19443994.2012.682965
[36] M. Zorko, R. Jerala, Alexidine and chlorhexidine bind to lipopolysaccharide and lipoteichoic acid and prevent cell activation by antibiotics, J. Antimicrob. Chemother., 62 (2008) 730-737. https://doi.org/10.1093/jac/dkn270
[37] A.D. Russell, F.R.C. Path, Chlorhexidine: Antibacterial action and bacterial resistance, Infection, 14 (1986) 212-215. https://doi.org/10.1007/bf01644264
[38] Z. Mohammadi, P.V. Abbott, The properties and applications of chlorhexidine in endodontics, Int. Endod. J., 42 (2009) 288-302. https://doi.org/10.1111/j.1365-2591.2008.01540.x
[39] T.H. Chong, F.S. Wong, A.G. Fane, The effect of imposed flux on biofouling in reverse osmosis: Role of concentration polarisation and biofilm enhanced osmotic pressure phenomena, J. Membr. Sci., 325 (2008) 840-850. https://doi.org/10.1016/j.memsci.2008.09.011
[40] I. Wiegand, K. Hilpert, R.E.W. Hancock, Agar and broth dilution methods to determine the minimal inhibitory concentration (MIC) of antimicrobial substances, Nat. Protoc., 3 (2008) 163-175. https://doi.org/10.1038/nprot.2007.521
[41] H.-S. Kim, S.-H. Lee, Y. Byun, H.-D. Park, 6-Gingerol reduces Pseudomonas aeruginosa biofilm formation and virulence via quorum sensing inhibition, Sci. Rep., 5 (2015) 8656-8666. https://doi.org/10.1038/srep08656
[42] T.S. Kim, P.F. Sun, Y.G. Park, H.D. Park, Effects of membrane and operational features on biofouling in a pressure retarded osmosis process, Desalin. Water Treat., 97 (2017) 79-86. https://doi.org/10.5004/dwt.2017.21661
[43] Q. She, X. Jin, C.Y. Tang, Osmotic power production from salinity gradient resource by pressure retarded osmosis: Effects of operating conditions and reverse solute diffusion, J. Membr. Sci., 401-402 (2012) 262-273. https://doi.org/10.1016/j.memsci.2012.02.014
[44] Q. She, D. Hou, J. Liu, K.H. Tan, C.Y. Tang, Effect of feed spacer induced membrane deformation on the performance of pressure retarded osmosis (PRO): Implications for PRO process operation, J. Membr. Sci., 445 (2013) 170-182. https://doi.org/10.1016/j.memsci.2013.05.061
[45] T.S. Kim, H.D. Park, Lauroyl arginate ethyl: An effective antibiofouling agent applicable for reverse osmosis processes producing potable water, J. Membr. Sci., 507 (2016) 24-33. https://doi.org/10.1016/j.memsci.2016.01.056
[46] A. Tiraferri, N.Y. Yip, A.P. Straub, S. Romero-Vargas Castrillon, M. Elimelech, A method for the simultaneous determination of transport and structural parameters of forward osmosis

membranes, J. Membr. Sci., 444 (2013) 523-538. https://doi.org/10.1016/j.memsci.2013.05.023
[47] J. Kim, B. Kim, D. Inhyuk Kim, S. Hong, Evaluation of apparent membrane performance parameters in pressure retarded osmosis processes under varying draw pressures and with draw solutions containing organics, J. Membr. Sci., 493 (2015) 636-644. https://doi.org/10.1016/j.memsci.2015.07.035
[48] M. Simoes, L.C. Simoes, S. Cleto, M.O. Pereira, M.J. Vieira, The effects of a biocide and a surfactant on the detachment of *Pseudomonas fluorescens* from glass surfaces, Int. J. Food Microbiol., 121 (2008) 335-341. https://doi.org/10.1016/j.ijfoodmicro.2007.11.041
[49] O. Habimana, A.J.C. Semião, E. Casey, The role of cell-surface interactions in bacterial initial adhesion and consequent biofilm formation on nanofiltration/reverse osmosis membranes, J. Membr. Sci., 454 (2014) 82-96. https://doi.org/10.1016/j.memsci.2013.11.043
[50] L.H. Kim, M.S. Shin, S.J. Kim, C.M. Kim, K.J. Chae, I.S. Kim, Potential effects of damaged *Pseudomonas aeruginosa* PAO1 cells on development of reverse osmosis membrane biofouling, J. Membr. Sci., 477 (2015) 86-92. https://doi.org/10.1016/j.memsci.2014.12.032
[51] L. Ni, J. Meng, X. Li, Y. Zhang, Surface coating on the polyamide TFC RO membrane for chlorine resistance and antifouling performance improvement, J. Membr. Sci., 451 (2014) 205-215. https://doi.org/10.1016/j.memsci.2013.09.040
[52] V.T. Do, C.Y. Tang, M. Reinhard, J.O. Leckie, Degradation of polyamide nanofiltration and reverse osmosis membranes by hypochlorite, Environ. Sci. Technol., 46 (2012) 852-859. https://doi.org/10.1021/es203090y
[53] W.R. Thelin, E. Sivertsen, T. Holt, G. Brekke, Natural organic matter fouling in pressure retarded osmosis, J. Membr. Sci., 438 (2013) 46-56. https://doi.org/10.1016/j.memsci.2013.03.020
[54] Q. She, L. Zhang, R. Wang, W.B. Krantz, A.G. Fane, Pressure-retarded osmosis with wastewater concentrate feed: Fouling process considerations, J. Membr. Sci., 542 (2017) 233-244. https://doi.org/10.1016/j.memsci.2017.08.022
[55] Q. She, X. Jin, Q. Li, C.Y. Tang, Relating reverse and forward solute diffusion to membrane fouling in osmotically driven membrane processes, Water Res., 46 (2012) 2478-2486. https://doi.org/10.1016/j.watres.2012.02.024
[56] S.E. Kwan, E. Bar-Zeev, M. Elimelech, Biofouling in forward osmosis and reverse osmosis: Measurements and mechanisms, J. Membr. Sci., 493 (2015) 703-708. https://doi.org/10.1016/j.memsci.2015.07.027
[57] M. Marroquin, T. Bruce, J. Pellegrino, S.R. Wickramasinghe, S.M. Husson, Characterization of asymmetry in microporous membranes by cross-sectional confocal laser scanning microscopy, J. Membr. Sci., 379 (2011) 504-515. https://doi.org/10.1016/j.memsci.2011.06.024
[58] C.Y. Tang, Q. She, W.C.L. Lay, R. Wang, A.G. Fane, Coupled effects of internal concentration polarization and fouling on flux behavior of forward osmosis membranes during humic acid filtration, J. Membr. Sci., 354 (2010) 123-133. https://doi.org/10.1016/j.memsci.2010.02.059
[59] F.A. Siddiqui, Q. She, A.G. Fane, R.W. Field, Exploring the differences between forward osmosis and reverse osmosis fouling, J. Membr. Sci., 565 (2018) 241-253. https://doi.org/10.1016/j.memsci.2018.08.034